A conserved mechanism for mitochondria-dependent dynein anchoring

Lauren M. Kraft and Laura L. Lackner*,†
Department of Molecular Biosciences, Northwestern University, Evanston, IL 60208

ABSTRACT **Mitochondrial anchors have functions that extend beyond simply positioning mitochondria. In budding yeast, mitochondria drive the assembly of the mitochondrial anchor protein Num1 into clusters, which serve to anchor mitochondria as well as dynein to the cell cortex. Here, we explore a conserved role for mitochondria in dynein anchoring by examining the tethering functions of the evolutionarily distant *Schizosaccharomyces pombe* Num1 homologue. In addition to its function in dynein anchoring, we find that *S. pombe* Num1, also known as Mcp5, interacts with and tethers mitochondria to the plasma membrane in *S. pombe* and *Saccharomyces cerevisiae*. Thus, the mitochondria and plasma membrane-binding domains of the Num1 homologues, as well as the membrane features these domains recognize, are conserved. In *S. pombe*, we find that mitochondria impact the assembly and cellular distribution of Num1 clusters and that Num1 clusters actively engaged in mitochondrial tethering serve as cortical attachment sites for dynein. Thus, mitochondria play a critical and conserved role in the formation and distribution of dynein-anchoring sites at the cell cortex and, as a consequence, impact dynein function. These findings shed light on an ancient mechanism of mitochondria-dependent dynein anchoring that is conserved over more than 450 million years of evolution, raising the intriguing possibility that the role mitochondria play in dynein anchoring and function extends beyond yeast to higher eukaryotes.**

Monitoring Editor
Gia Voeltz
University of Colorado, Boulder

Received: Jul 25, 2018
Revised: Dec 5, 2018
Accepted: Jan 8, 2019

INTRODUCTION

Mitochondrial anchors influence the overall structure and cellular distribution of the mitochondrial network. Anchors function to keep mitochondria at regions where there is a high demand for mitochondrial activity and impact the quantity and quality of mitochondria that are inherited by daughter cells (McFaline-Figueroa *et al.*, 2011; Klecker *et al.*, 2013; Schwarz, 2013; Pernice *et al.*, 2016; Sheng, 2017). Thus, anchor-mediated positioning of mitochondria at specific places and specific times is intimately tied to cellular function and physiology (Pernice *et al.*, 2017; Kraft and Lackner, 2018).

In budding yeast, Num1 anchors mitochondria as well as dynein to the cell cortex. For its role in mitochondrial anchoring, Num1 serves as the core component of the mitochondria–ER–cortex anchor (MECA), which functions to tether mitochondria to the plasma membrane (PM) and impacts the distribution and inheritance of the organelle (Cerveny *et al.*, 2007; Tang *et al.*, 2012; Klecker *et al.*, 2013; Lackner *et al.*, 2013). As a dynein anchor, Num1 functions in one of two partially redundant nuclear migration pathways. Specifically, Num1 serves as a cortical attachment site for dynein, where, once anchored, dynein captures and walks along astral microtubules to help orient the mitotic spindle (Kormanec *et al.*, 1991; Eshel *et al.*, 1993; Adames and Cooper, 2000; Heil-Chapdelaine *et al.*, 2000; Farkasovsky and Kuntzel, 2001; Markus and Lee, 2011). Although dynein is not required for Num1-mediated mitochondrial anchoring (Cerveny *et al.*, 2007; Tang *et al.*, 2012; Lackner *et al.*, 2013), mitochondria drive the assembly of Num1 clusters, which in turn serve to stably anchor the organelle itself as well as dynein to the PM. When mitochondria-driven assembly of Num1 clusters is disrupted, defects in dynein-mediated spindle positioning are observed (Kraft and Lackner, 2017; Schmit *et al.*, 2018). The functional and physiological significance of why mitochondria are used to

This article was published online ahead of print in MBoC in Press (http://www.molbiolcell.org/cgi/doi/10.1091/mbc.E18-07-0466) on January 16, 2019.

L.M.K conducted the experiments and along with L.L.L. conceived the study, designed experiments, and wrote the paper.

†ORCID: orcid.org/0000-0003-0311-5199

*Address correspondence to: Laura L. Lackner (Laura.Lackner@northwestern.edu).

Abbreviations used: AID, auxin-inducible degron; CC, coiled-coil; CL, cardiolipin; ER, endoplasmic reticulum; MECA, mitochondria-ER-cortex-anchor; mitoAID, conditional mitochondrial inheritance mutant; PA, phosphatidic acid; PG, phosphatidylglycerol; PH, pleckstrin homology; PM, plasma membrane; PS, phosphatidylserine; ScNum1, *S. cerevisiae* Num1; SpNum1, *S. pombe* Num1.

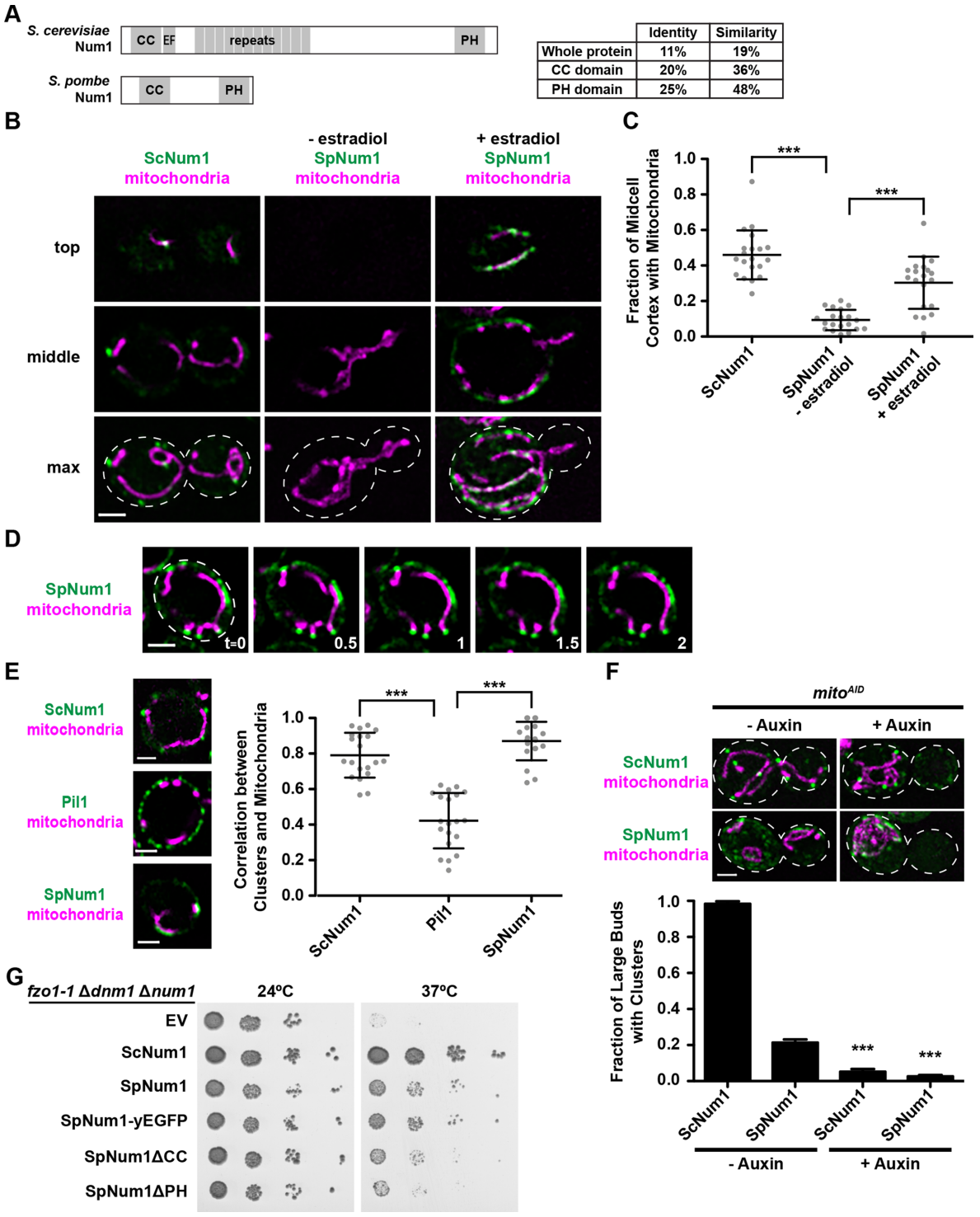

FIGURE 1: SpNum1 tethers mitochondria to the plasma membrane in budding yeast. (A) Schematics of ScNum1 and SpNum1 and their degree of similarity and identity. Schematics are drawn to scale. Paircoil2 was used to specifically define the CC domain of SpNum1 as residues 132–360, which will be referred to as SpNum1CC. CC, coiled-coil; EF, EF hand-like motif; PH, pleckstrin homology domain. (B, C) Cells expressing mitoRED and ScNum1-yEGFP or estradiol-regulated SpNum1-yEGFP grown in the presence or absence of estradiol, as indicated, were analyzed by fluorescence microscopy. Whole cell, maximum intensity projections as well as single focal planes from the top and middle of the cell are shown (B). The cell cortex is outlined with a dashed white line. Bar = 2 μm. The graph shows quantification of the fraction of the cell cortex at midcell that is occupied by mitochondria (C). The mean ± SD is shown; $n = 20$ cell per strain. ***, $p < 0.0001$. (D) Cells expressing mitoRED and estradiol-regulated SpNum1-yEGFP were grown in the presence of estradiol and analyzed by fluorescence microscopy. A single focal plane is shown. The cell cortex is outlined with a dashed white line. Bar = 2 μm. t = minutes. (E) Cells expressing mitoRED and ScNum1-yEGFP, Pil1-yEGFP, or estradiol-regulated SpNum1-yEGFP grown in the presence of estradiol were imaged and analyzed by fluorescence

drive the formation of cortical attachment sites for dynein has yet to be determined.

For its role in mitochondrial anchoring, Num1 interacts with mitochondria and the PM via two distinct lipid-binding domains. A membrane-binding region within the N-terminal coiled-coil (CC) domain of Num1 interacts directly with the mitochondrial outer membrane exhibiting a preference for the mitochondrial specific lipid cardiolipin (CL; Tang *et al.*, 2012; Lackner *et al.*, 2013; Ping *et al.*, 2016). The CC domain is also required for the interaction with dynein (Tang *et al.*, 2012). The C-terminal pleckstrin homology (PH) domain interacts with $PI_{4,5}P_2$ in the PM (Farkasovsky and Kuntzel, 1995; Yu *et al.*, 2004; Tang *et al.*, 2009). The endoplasmic reticulum (ER) is present at sites of Num1-mediated mitochondria–PM tethering, but the mechanism of interaction is poorly understood (Lackner *et al.*, 2013; Chao *et al.*, 2014). The 313 kDa Num1 protein also contains an EF hand-like motif and a region of twelve 64 amino acid repeats, the functions of which have yet to be described (Figure 1A; Kormanec *et al.*, 1991). Although the CC and PH domains are present in Num1 homologues from other fungal species, the repeat region, EF hand-like motif, and overall size of the protein are less conserved (Saito *et al.*, 2006; Yamashita and Yamamoto, 2006).

In the case of the evolutionarily distant *Schizosaccharomyces pombe* Num1 homologue (SpNum1), also referred to as Mcp5, both the CC and PH domains are required to anchor dynein to the cell cortex. Similar to *Saccharomyces cerevisiae* Num1 (ScNum1), the CC domain of SpNum1 is required for its interaction with dynein, and the PH domain binds to $PI_{4,5}P_2$ in the PM (Saito *et al.*, 2006; Yamashita and Yamamoto, 2006; Thankachan *et al.*, 2017). In contrast to the mitotic role of ScNum1-anchored dynein in budding yeast, SpNum1-anchored dynein is required for nuclear oscillation during the early stages of *S. pombe* meiosis. During meiotic prophase, the nucleus migrates back and forth between the two poles of the cell in what is referred to as a horsetail movement. Nuclear oscillation is driven by the pulling of astral microtubules emanating from the spindle pole body by cortically anchored dynein at the opposite end of the cell (Yamamoto *et al.*, 1999, 2001). Nuclear movement facilitates efficient homologous chromosome pairing and meiotic recombination (Yamamoto *et al.*, 1999; Saito *et al.*, 2006; Yamashita and Yamamoto, 2006). Consistent with a function in meiosis, the expression of both SpNum1 and dynein is restricted to meiotic prophase I (Yamamoto *et al.*, 1999; Mata *et al.*, 2002; Saito *et al.*, 2006; Yamashita and Yamamoto, 2006).

Although clusters of SpNum1 at the cell cortex have been shown to anchor dynein, what drives the formation of these clusters is unknown. The dynein-anchoring functions of the CC and PH domains are conserved between the two Num1 homologues. This raises the intriguing, yet unexplored, possibility that SpNum1 also tethers mitochondria and the interaction with mitochondria impacts SpNum1 cluster formation and, consequently, dynein anchoring. To further investigate the function and mechanism of Num1-mediated anchoring as well as the possibility of a conserved role for mitochondria in dynein anchoring, we examined the tethering functions of SpNum1. We find that SpNum1 interacts directly with mitochondria and tethers mitochondria to the PM in both *S. pombe* and *S. cerevisiae*. Our data indicate that mitochondria impact the distribution of SpNum1 clusters along the cell cortex, and that, in *S. pombe*, dynein is anchored by Num1 clusters that have been assembled by and are actively tethering mitochondria. Given the evolutionary distance between *S. cerevisiae* and *S. pombe*, which is estimated to be 450–1000 million years (Sipiczki, 2000; Heckman *et al.*, 2001), our findings shed light on an ancient mechanism of mitochondria-dependent dynein anchoring.

RESULTS

S. pombe Num1 anchors mitochondria to the PM in *S. cerevisiae*

Mitochondrial tethering mediated by ScNum1 requires two membrane-binding domains within the protein, the CC and PH domains (Yu *et al.*, 2004; Tang *et al.*, 2009; Ping *et al.*, 2016). If the CC and PH domains recognize conserved features on the membranes to which they bind and are sufficient for mitochondrial tethering, we reasoned that Num1 homologues, such as SpNum1, should be able to anchor mitochondria to the PM in *S. cerevisiae*. Although the overall homology between ScNum1 and SpNum1 is weak, comparisons of the CC and PH domains of each protein reveal a higher degree of similarity and identity (Figure 1A).

To test whether SpNum1 is able to anchor mitochondria to the PM in budding yeast, we replaced the *ScNUM1* coding region with *SpNUM1-yEGFP* expressed from an estradiol-driven promoter. In the absence of estradiol, *SpNUM1-yEGFP* cells exhibited noncortical, collapsed mitochondrial networks that phenocopy Δ*num1* cells (Figure 1B; Cerveny *et al.*, 2007; Klecker *et al.*, 2013; Lackner *et al.*, 2013). In the presence of estradiol, SpNum1 formed clusters that colocalized with mitochondria at the cell cortex similar to ScNum1, and the cortical distribution of mitochondria was restored (Figure 1B). Indeed, a larger fraction of the cell cortex at midcell was occupied by mitochondria in cells expressing SpNum1 (+estradiol) compared with cells lacking SpNum1 (–estradiol), indicating that SpNum1 is able to tether mitochondria to the PM (Figure 1C). In comparison to the distinct clusters formed by ScNum1, SpNum1 appeared to accumulate into broader patches at tethering sites. However, as the steady-state levels of SpNum1 were twofold greater than ScNum1, we were not able to make any conclusions about the assembly properties of the proteins.

When examined over time, the most intense and stable accumulations of SpNum1 were persistently associated with mitochondria (Figure 1D). These data suggest that, similar to ScNum1, the ability of SpNum1 to form clusters is dependent on an interaction with mitochondria (Kraft and Lackner, 2017). To further support this idea, we quantified the correlation between SpNum1 clusters and mitochondria along the midcell circumference of a cell (Figure 1E). ScNum1 and Pil1, the core component of a discrete PM compartment called the eisosome (Walther *et al.*, 2006), were used as positive and negative controls, respectively. We found the correlation between ScNum1 clusters and the presence of mitochondria to be high,

microscopy. The correlation between accumulations of ScNum1, Pil1, or SpNum1 and mitochondria at the cell cortex is shown as the mean ± SD. $n = 20$ cells per strain. ***, $p < 0.0001$. (F) *mito*^{AID} cells expressing ScNum1-yEGFP or estradiol-regulated SpNum1-yEGFP grown in the presence of estradiol along with mitoRED were grown in the absence or presence of auxin and visualized by fluorescence microscopy. Whole cell, maximum intensity projections are shown. The cell cortex is outlined with a dashed white line. Bar = 2 µm. The presence of assembled Num1 in large buds was quantified. Large buds were classified as having a bud/mother diameter ratio of ≥1/3. $n = 3$ independent experiments of ≥72 cells for each bud size. The graph shows the mean ± SD. The *p* values are in comparison to the same genotype grown in the absence of auxin. ***, $p < 0.0001$. (G) Serial dilutions of *fzo1-1* Δ*dnm1* Δ*num1* cells expressing the indicated proteins were grown at 24°C or 37°C, as indicated. EV, empty vector.

consistent with previous results (Kraft and Lackner, 2017). In contrast, the clusters of Pil1 weakly correlated with the presence of mitochondria. Similar to ScNum1 clusters, SpNum1 clusters highly correlated with the presence of mitochondria (Figure 1E). These data are consistent with the idea that the formation of SpNum1 clusters depends on an interaction with mitochondria.

To further support the idea that SpNum1 cluster formation is mitochondria dependent, we examined the ability of SpNum1 to form clusters in buds that lack mitochondria using a conditional mitochondrial inheritance strain, *mito*^{AID} (Kraft and Lackner, 2017). This strain lacks Ypt11, one of the two adaptors required for Myo2-driven transport of mitochondria to the bud, and expresses the other adaptor, Mmr1, as a fusion to an auxin-inducible degron (AID). Consequently, the inheritance of mitochondria by buds in *mito*^{AID} cells is inhibited in the presence of auxin (Figure 1F, cell images; Kraft and Lackner, 2017). As a control, we examined ScNum1 cluster formation in *mito*^{AID} cells. Consistent with mitochondria-driven assembly, the addition of auxin significantly reduced the number of large buds in which ScNum1 clusters were observed (Figure 1F). In comparison to ScNum1 clusters, SpNum1 clusters were observed in a smaller fraction of large buds in the absence of auxin for reasons that are at this point unclear. Importantly, however, the addition of auxin significantly reduced the number of large buds in which SpNum1 clusters were observed (Figure 1F). These results further support the idea that SpNum1 cluster formation is dependent on mitochondria.

We also examined the relationship between SpNum1 clusters and the ER and found that, in contrast to ScNum1 clusters, which colocalize with cortical ER (Lackner *et al*., 2013; Chao *et al*., 2014), SpNum1 clusters localized to ER-free regions of the PM (Supplemental Figure S1A). Thus, the ability to associate with mitochondria and the PM is conserved between the two Num1 homologues, but the ER association is not.

The mitochondrial tethering activity of ScNum1 is essential in the absence of the mitochondrial division and fusion proteins, Dnm1 and Fzo1, respectively (Lackner *et al*., 2013). To further confirm the tethering activity of SpNum1 in budding yeast, we tested whether the expression of SpNum1 was able to rescue the severe growth defect of *fzo1-1* Δ*dnm1* Δ*num1* cells grown at the nonpermissive temperature for the *fzo1-1* temperature-sensitive allele (Hermann *et al*., 1998). Consistent with the ability of SpNum1 to tether mitochondria, we found that *fzo1-1* Δ*dnm1* Δ*num1* cells expressing full-length SpNum1 grew better than cells containing an empty vector control or cells expressing constructs lacking the CC and PH domains (Figure 1G). Together, the above results indicate that SpNum1 is able to tether mitochondria to the PM in budding yeast and suggest that the CC and PH domains play roles in tethering.

The ability of the Num1 CC domain to bind lipid membranes is conserved

We next sought to determine whether, similar to ScNum1, the CC domain of SpNum1 interacts with mitochondria. To test this, we first examined whether the CC domain of SpNum1 alone interacts with mitochondria in cells. We expressed SpNum1CC (amino acids 132–360) as a yEGFP fusion from the endogenous *ScNUM1* locus in cells also expressing mitoRED. These cells lack a full-length version of Num1, and, therefore, mitochondria tend to exhibit a collapsed, noncortical distribution. We observed an enrichment of SpNum1CC-yEGFP on mitochondria in addition to a diffuse cytosolic pool of the protein (Figure 2, A and B). The average peak intensity of the SpNum1CC-yEGFP signal on mitochondria (1693 ± 673, $n = 20$) was significantly greater than the average peak intensity of mitochondrial autofluorescence under the same imaging conditions (455 ± 673, $n = 20$). These data are consistent with the idea that SpNum1CC is able to interact with mitochondria in vivo.

To further support this idea, we anchored SpNum1CC to the cell cortex using the GFP-αGFP nanobody targeting system we developed (Schmit *et al*., 2018), and we examined the ability of artificially anchored SpNum1CC to restore the cortical localization of mitochondria. Specifically, we expressed SpNum1CC-yEGFP in Δ*num1* cells engineered to express Pil1 as an αGFP nanobody fusion (Pil1-αGFP) from the endogenous *PIL1* locus. The αGFP nanobody is an ~16 kDa, monomeric, single domain antibody that binds GFP with high affinity (Muyldermans, 2013; Fridy *et al*., 2014). In the presence of Pil1-αGFP, SpNum1CC-yEGFP localized to discrete clusters at the cell cortex, indicating the protein was effectively targeted to eisosomes (Figure 2C). We found that mitochondria were persistently localized to a subset of Pil1-associated SpNum1CC-yEGFP clusters (Figure 2C). Consistent with the ability of artificially anchored SpNum1CC-yEGFP to tether mitochondria to the cell cortex, a larger fraction of the cell cortex at midcell was occupied by mitochondria in Δ*num1* Pil1-αGFP cells expressing SpNum1CC-yEGFP compared with Δ*num1* Pil1-αGFP cells expressing yEGFP alone (Figure 2D). These results indicate that SpNum1CC, when cortically anchored to the cell cortex by artificial means, is able to interact with and tether mitochondria to the cell cortex.

We next examined the ability of SpNum1CC to interact directly with phospholipid membranes in vitro. We purified SpNum1CC from *Escherichia coli* and subjected the pure protein to liposome flotation assays. The liposomes used were composed of soybean polar lipid extract supplemented with either 6 or 17 mol% CL, which approximate the composition of the mitochondrial outer membrane and contact sites between the mitochondrial inner and outer membranes, respectively (Simbeni *et al*., 1991; Zinser and Daum, 1995). Recombinant SpNum1CC associated with liposomes, and this interaction was enhanced with increasing amounts of CL (Figure 2, E and F). To further examine the phospholipid binding activity of SpNum1CC, we replaced the 17 mol% CL with 34 mol% phosphatidic acid (PA), phosphatidylglycerol (PG), or phosphatidylserine (PS), keeping the overall net charge of the liposomes constant. The headgroup of CL has two negatively charged phosphates and the headgroups of PA, PG, and PS have one negatively charged phosphate. Although SpNum1CC associated with liposomes containing 34 mol% PA, PG, and PS (Supplemental Figure S2), the fraction SpNum1CC associated with liposomes was significantly reduced in comparison to liposomes containing 17 mol% CL (~0.67, 0.65, and 0.37, for PA, PG, and PS, respectively, in comparison to ~0.89 for CL), indicating that it is not the negative charge of the headgroup alone that facilitates the liposome interaction and that other properties of the phospholipids contribute. Interestingly, PA and PG have both been proposed to compensate for CL in cells (Chang *et al*., 1998; Chen *et al*., 2010; Connerth *et al*., 2012), suggesting that the phospholipids have some functional overlap. Together, our in vivo and in vitro results, in combination with previous studies, indicate that the CC domains of SpNum1 and ScNum1 interact with mitochondria via a conserved phospholipid membrane-binding mechanism.

S. pombe Num1 associates with mitochondria during fission yeast meiosis

Our data indicate that SpNum1 is able to tether mitochondria to the cell cortex in budding yeast, raising the question of whether the protein performs a similar function in fission yeast. To test this idea, we examined the localization of SpNum1 relative to mitochondria during fission yeast meiosis. Haploid cells, both expressing SpNum1-yEGFP from the endogenous locus along with mitoRED, were

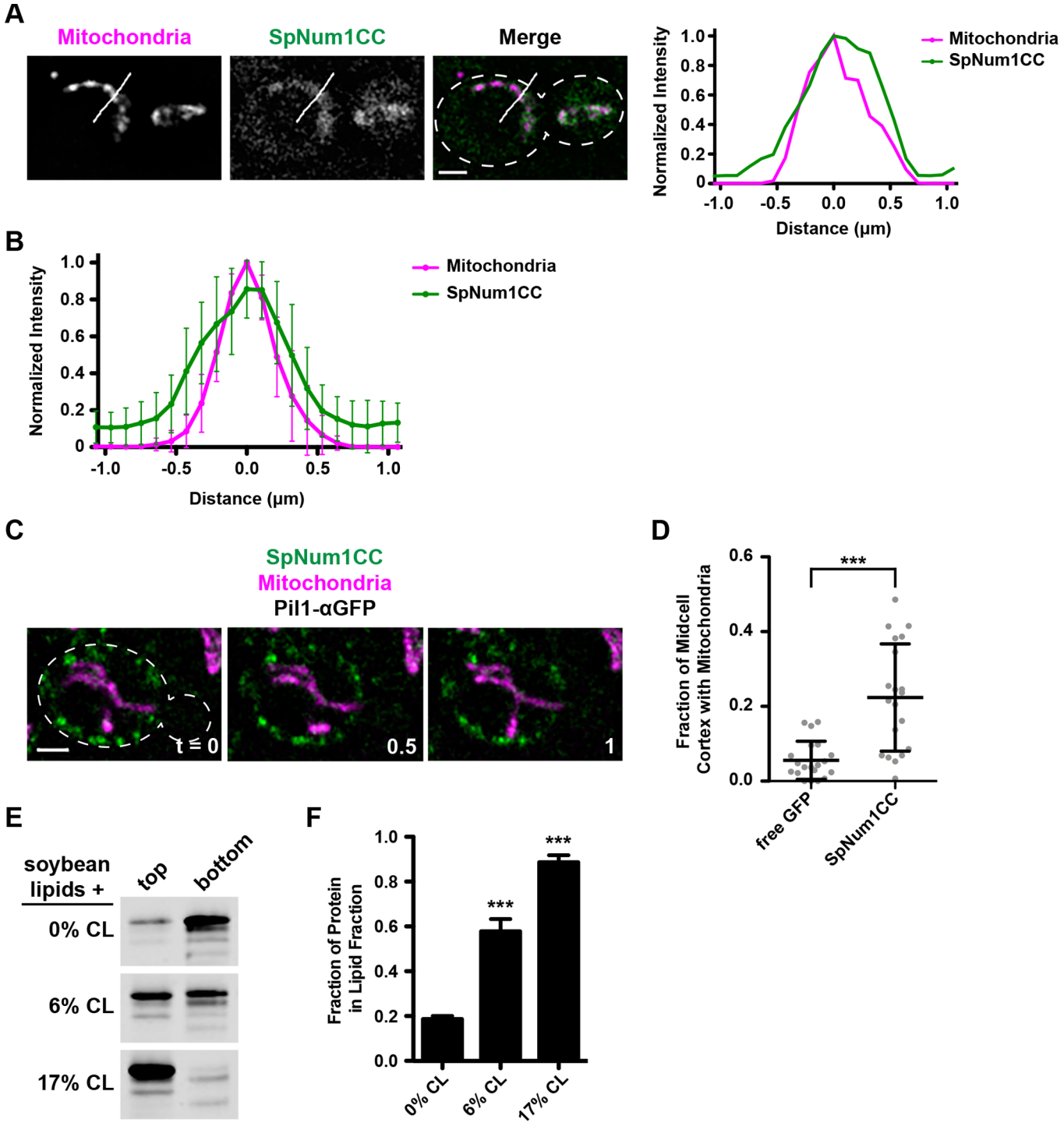

FIGURE 2: SpNum1CC interacts with mitochondria. (A, B) Cells expressing ScNum1CC-yEGFP from the endogenous Num1 locus and mitoRED were analyzed by fluorescence microscopy. A single focal plane is shown. The cell cortex is outlined with a dashed white line. Bar = 2 μm. The graphs show normalized fluorescence intensities of mitoRED (magenta) and ScNum1CC-yEGFP (green) along a line drawn perpendicular to a mitochondrial tubule for the corresponding image (A, white line) and the mean ± SD of 20 line scans (B). The position of peak mitoRED intensity was set at 0 μm. (C, D) SpNum1CC-yEGFP and yEGFP were expressed in Δ*num1* Pil1-αGFP cells also expressing mitoRED, and the cells were imaged by fluorescence microscopy. A maximum intensity projection of three focal planes is shown for cells expressing SpNum1CC-yEGFP (C). The cell cortex is outlined with a dashed white line. Bar = 2 μm. *t* = minutes. The graph shows quantification of the fraction of the cell cortex at midcell that is occupied by mitochondria (D). The mean ± SD is shown; *n* = 20 cells per strain. ***, $p < 0.0001$. (E, F) SpNum1CC (3 μM) was incubated with soybean liposomes spiked with 0, 6, or 17 mol% CL. The association of the protein with liposomes was assessed by its ability to float with liposomes, as indicated by the amount of protein in the top fraction of the gradient. The fraction of protein found in the top fraction is shown in D as the mean ± SEM; *n* = 3 independent experiments. The *p* values are in comparison to 0% CL. ***, $p < 0.0001$.

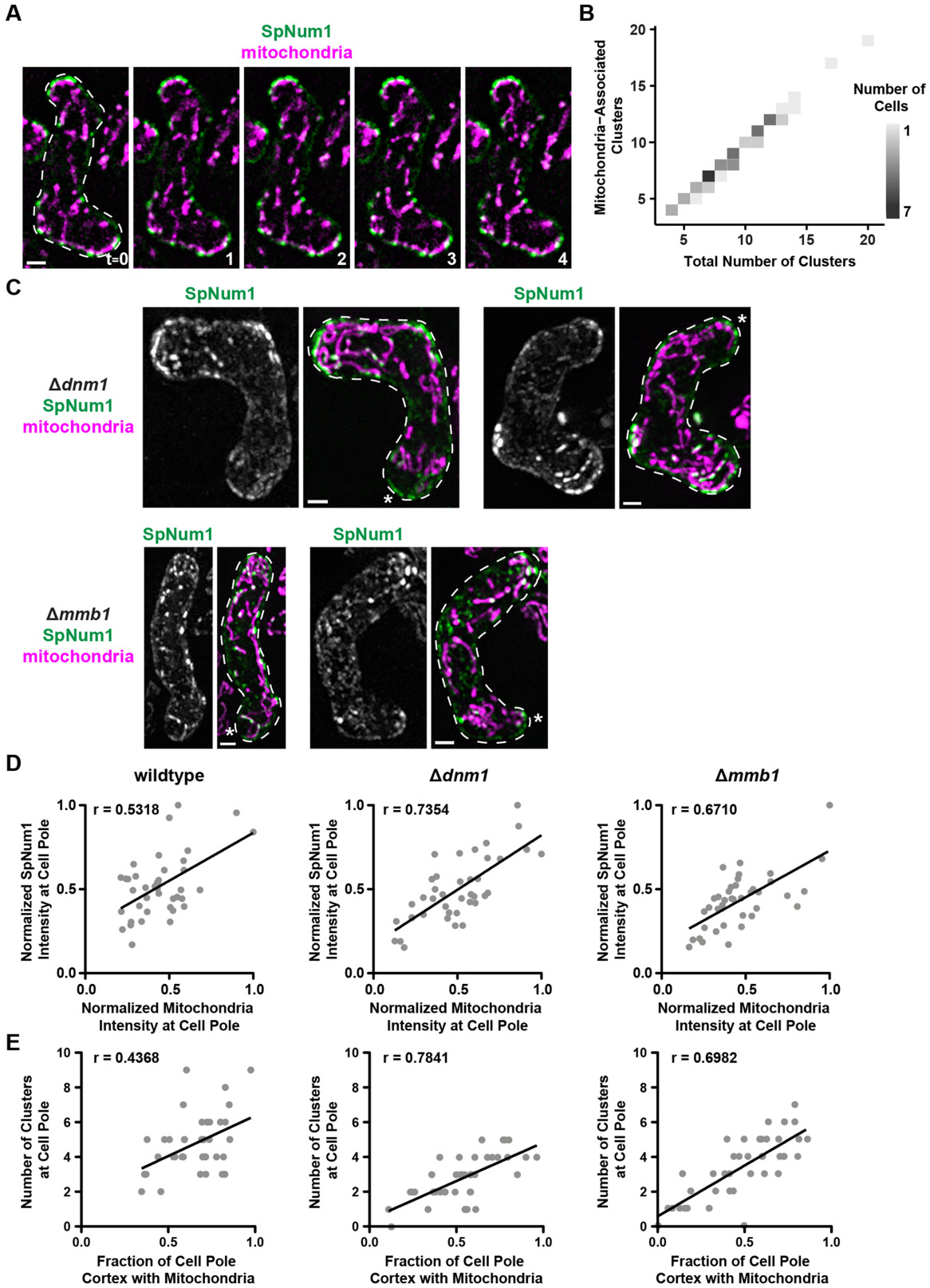

FIGURE 3: *S. pombe* Num1 associates with mitochondria during fission yeast meiosis. (A, B) Wild-type meiotic *S. pombe* cells expressing SpNum1-yEGFP and mitoRED were analyzed by fluorescence microscopy. Maximum intensity projections of two focal planes are shown (A). The cell cortex is outlined with a dashed white line. Bar = 2 μm. *t* = minutes. Quantification of the number of mitochondria-associated SpNum1 clusters per midcell slice vs. the total number of clusters per midcell slice is shown (B). The color of each rectangle represents the number of cells, as indicated by the key. A total of 54 cells and 496 clusters were quantified. (C–E) Δ*dnm1* and Δ*mmb1* meiotic *S. pombe* cells expressing SpNum1-yEGFP and mitoRED were analyzed by fluorescence microscopy. Whole cell, maximum

mated, and meiotic cells were imaged over time. In meiotic cells, SpNum1 localized along the cortex as well as in clusters enriched at the poles, as previously described (Saito *et al.*, 2006; Yamashita and Yamamoto, 2006; Thankachan *et al.*, 2017). Interestingly, there was a striking colocalization between SpNum1 clusters and mitochondria, which persisted over time (Figure 3A). A cluster is defined as an accumulation of SpNum1 above the background signal that persisted for >1.5 min. In the vast majority of cells, the number of total and mitochondria-associated clusters in a given single focal plane were equivalent, with 97.2% of total clusters being mitochondria associated (Figure 3B). Thus, very few non-mitochondria-associated clusters were observed. Similar results were observed in cells lacking dynein (Supplemental Figure S3; 97.6% of total clusters were mitochondria associated), indicating that the interaction between SpNum1 and mitochondria does not depend on dynein. We also examined the relationship between SpNum1 and the ER. As observed in *S. cerevisiae*, SpNum1 clusters did not colocalize with the ER in *S. pombe* (Supplemental Figure S1B).

The distribution of Num1 clusters in *S. pombe* is dependent on mitochondria

In *S. pombe*, SpNum1 clusters not associated with mitochondria were rarely observed, providing additional support for the idea that SpNum1 cluster assembly may depend on an interaction with mitochondria. To further test this idea in *S. pombe*, we examined the localization of SpNum1 in cells lacking either Mmb1, a protein that links mitochondria to microtubules, or Dnm1, a dynamin-related protein required for mitochondrial division (Bleazard *et al.*, 1999; Guillou *et al.*, 2005; Jourdain *et al.*, 2009; Fu *et al.*, 2011). Mitochondrial distribution is disrupted in these cells, resulting in regions of the cell with reduced mitochondrial content. If mitochondria are required for SpNum1 clustering, we would expect to see fewer clusters in these regions. We mated Δ*mmb1* or Δ*dnm1* haploids expressing SpNum1-yEGFP as well as mitoRED and observed mitochondrial distribution was disrupted in meiotic cells, with a small fraction of cells having poles with reduced mitochondrial content. When compared with poles that contained mitochondria, poles with reduced mitochondrial content had fewer SpNum1 clusters, which were defined as an accumulation of SpNum1 above the background signal that persisted for >1.5 min (Figure 3C). We quantified the correlation between SpNum1 clusters and mitochondrial content at cell poles observed in Figure 3C in two ways. Using sum intensity maximum projections, we quantified the total fluorescence intensity of SpNum1 and mitochondria at the cell poles. We found that the fluorescence intensity of SpNum1 and mitochondria were strongly correlated; less SpNum1 intensity was observed in poles with reduced mitochondrial content (Figure 3D). We also quantified the number of SpNum1 clusters and the fraction of the cortex occupied by mitochondria at cell poles in a midcell plane and found a strong correlation between the two; fewer Num1 clusters were observed in poles that had fewer mitochondria present along the cortex (Figure 3E). These data further support the idea that SpNum1 clustering and distribution are dependent on mitochondria.

Num1 can simultaneously anchor mitochondria and dynein to the cell cortex in *S. pombe*

During nuclear oscillation, dynein is observed at multiple locations in the cell (Yamamoto *et al.*, 1999). As depicted in Figure 4A, dynein is observed on the spindle pole body (arrowhead), along microtubules (asterisks), and in a bright spot at the cell cortex in front of the moving nucleus (arrow). The spindle pole body moves toward and eventually appears to colocalize with the bright spot of cortically anchored dynein (Yamamoto *et al.*, 1999), which is anchored to the PM by clustered SpNum1 (Saito *et al.*, 2006; Yamashita and Yamamoto, 2006; Thankachan *et al.*, 2017). Interestingly, our data indicate that mitochondria are persistently localized to the vast majority of SpNum1 clusters, suggesting that SpNum1 can simultaneously anchor mitochondria and dynein. To test this idea, we examined the relationship between cortical dynein spots and mitochondria in meiotic cells. We mated haploid cells expressing the dynein heavy chain (Dhc1) as a yEGFP fusion from its endogenous locus along with mitoRED. In meiotic cells undergoing nuclear oscillations, we observed mitochondria present at sites where dynein was anchored to the cortex (Figure 4B, arrows). Specifically, we found that 89.6% of cortical dynein spots (86 out of 96) colocalized with mitochondria, indicating that a SpNum1 cluster can simultaneously anchor mitochondria and dynein. To further confirm the presence of mitochondria at sites of dynein anchoring, we examined the relationship between cortically anchored dynein and mitochondria in the small fraction of poles in meiotic Δ*mmb1* and Δ*dnm1* cells that have reduced mitochondrial content and, therefore, large regions of the cell cortex devoid of mitochondria. Importantly, the vast majority of dynein-anchoring events at poles with reduced mitochondrial content were observed at sites on the cortex where mitochondria were present (Figure 4C, arrows; Δ*mmb1* cells are shown); 93.8% of cortical dynein spots (45 out of 48) colocalized with mitochondria. Together, these results support the idea that dynein is anchored by SpNum1 clusters that are actively tethering mitochondria and highlight the role mitochondria play in the distribution of cortical attachment sites for dynein.

DISCUSSION

Here we provide evidence that a role for mitochondria in dynein anchoring is conserved between two evolutionarily distant yeast species, *S. cerevisiae* and *S. pombe,* and therefore, over 450–1000 million years of evolution (Sipiczki, 2000; Heckman *et al.*, 2001). These findings raise the intriguing possibility that a role for mitochondria in dynein anchoring and function extends beyond yeast to higher eukaryotes. Why mitochondria are used to drive the formation of cortical attachment sites for dynein is still an outstanding question.

In *S. cerevisiae* and *S. pombe*, Num1 is the central player in mitochondria-dependent dynein anchoring. Our data, and that of others, demonstrate that the CC and PH domains of the Num1 homologues recognize conserved features within the mitochondrial and PMs, respectively. The PH domain recognizes $PI_{4,5}P_2$ in the PM (Farkasovsky and Kuntzel, 1995; Yu *et al.*, 2004; Tang *et al.*, 2009), and the CC domain likely recognizes a membrane structure that is

intensity projections are shown (C). The cell cortex is outlined with a dashed white line. Bar = 2 μm. * indicates poles with reduced mitochondrial content. The total fluorescence intensities of mitoRED and SpNum1-yEGFP at the poles of wild-type, Δ*dnm1*, and Δ*mmb1* meiotic *S. pombe* cells were quantified from sum intensity projections as described in *Materials and Methods* and plotted (D). The number of SpNum1 clusters and the fraction of the cortex occupied by mitochondria at cell poles in a midcell plane were quantified as described in *Materials and Methods* and plotted (E). $n = 40$ poles per genotype; Pearson correlation coefficient, r, is shown. $p < 0.0005$ for all correlations.

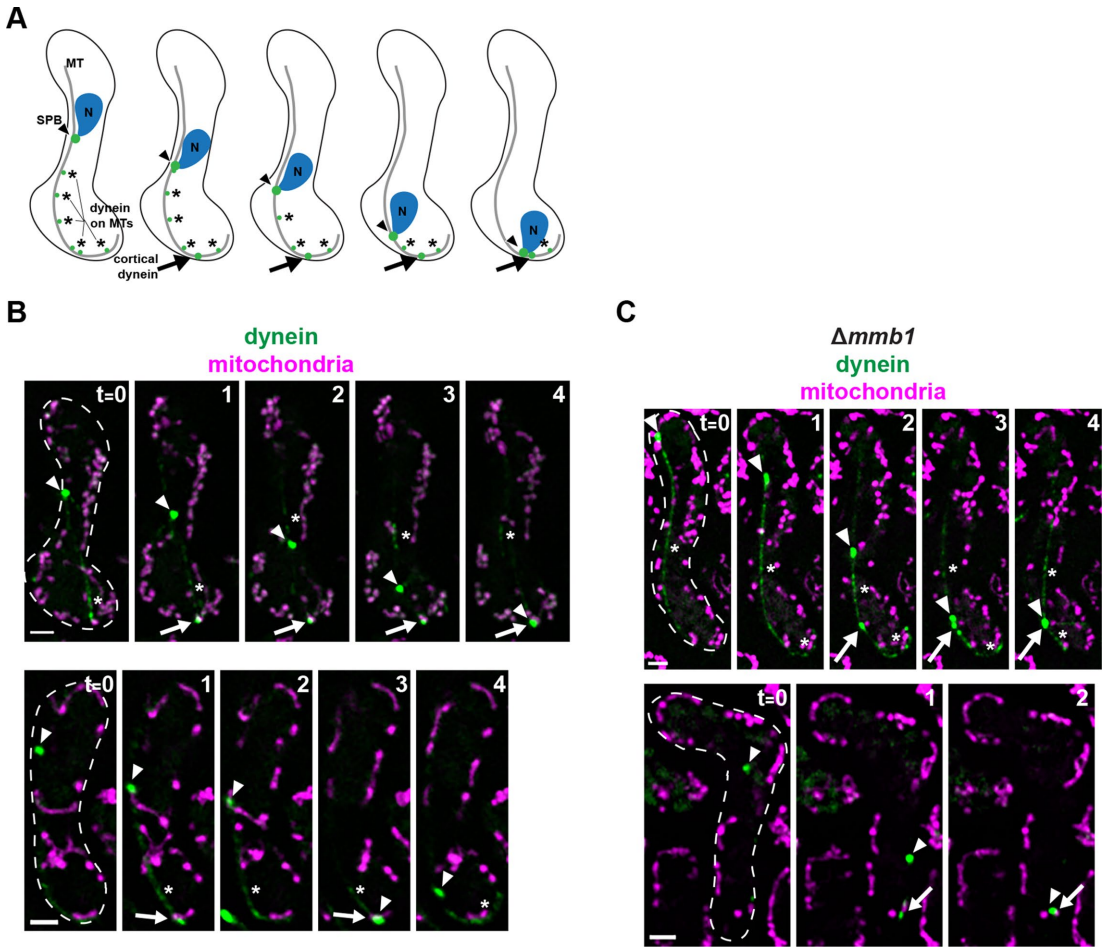

FIGURE 4: Mitochondria are present at sites of cortical dynein anchoring in meiotic fission yeast. (A) Schematic of dynein localization during nuclear oscillation in *S. pombe*. Dynein is observed on the spindle pole body (arrowhead), along microtubules (asterisks), and in a bright spot at the cell cortex in front of the moving nucleus (arrow). The cortical spot of dynein (arrow) is anchored to the PM by clustered SpNum1. The spindle pole body moves toward and eventually colocalizes with cortically anchored dynein. SPB, spindle pole body; MT, microtubule; N, nucleus. (B, C) Meiotic wild-type (B) or Δ*mmb1* (C) *S. pombe* cells expressing Dhc1-yEGFP and mitoRED were analyzed by fluorescence microscopy. Maximum intensity projections of five focal planes are shown. Dynein at the spindle pole body, along microtubules, and anchored at the cortex is indicated as in panel A. The cell cortex is outlined with a dashed white line. Bar = 2 μm. *t* = minutes. For Δ*mmb1* cells, the nucleus is moving toward the pole with reduced mitochondrial content.

formed and/or maintained by CL and additional factors, such as proteins and other phospholipids that reside in the mitochondrial outer membrane or mitochondrial outer-inner membrane contact sites (Figure 2 and Supplemental Figure S2; Ping *et al.*, 2016). Although the ability of SpNum1 to bind specific membranes is retained in budding yeast, SpNum1 does not appear to be functional in the *S. cerevisiae* dynein nuclear inheritance pathway. Specifically, we found that cells expressing SpNum1 in place of ScNum1 exhibited a severe growth defect in the absence of Kar9, an essential component of a partially redundant nuclear migration pathway in budding yeast (Supplemental Figure S4; Miller and Rose, 1998). Defects in the dynein nuclear inheritance pathway are lethal or severely synthetic sick in the absence of *KAR9*. Although the degree of similarity and identity between the CC and PH domains of the Num1 homologues is higher than other regions of the proteins, it is still relatively low. This likely explains the inability of SpNum1 to rescue the dynein pathway in budding yeast. In contrast, it is not uncommon for membrane-binding domains with similar structure and lipid-binding preferences, such as PH and BAR domains, to have low sequence identity (Ren *et al.*, 2006; Lemmon, 2010). This makes it challenging to identify functional homologues of Num1, that is, proteins or protein complexes that bind and tether mitochondria and the PM, in other organisms.

Interestingly, unlike the mitochondria-ER-PM contact sites formed by ScNum1, the ER is not present at mitochondrial tethering sites in *S. pombe*. Previous work indicates that the region of ScNum1 that mediates the interaction with the ER lies between the CC and PH domains (Lackner *et al.*, 2013; Chao *et al.*, 2014), and therefore, in the less conserved regions of the protein. In contrast to ScNum1, which forms stable membrane contacts throughout the mitotic cell cycle (Kraft and Lackner, 2017), SpNum1 is expressed and functions in a very specific stage of meiosis (Mata *et al.*, 2002; Saito *et al.*, 2006; Yamashita and Yamamoto, 2006). In this context, we speculate that the function of SpNum1 may be limited to its role in serving as a cortical anchor for dynein, whereas ScNum1 has functions beyond dynein anchoring. Indeed, ScNum1 is required for proper mitochondrial distribution and inheritance (Cerveny *et al.*, 2007; Klecker *et al.*, 2013; Lackner *et al.*, 2013), and *NUM1* exhibits genetic interactions

distinct from that of *DYN1* (Costanzo *et al.*, 2010; Hoppins *et al.*, 2011). Thus, the stable mitochondria-ER-PM contact sites formed by ScNum1 have additional, yet to be determined functions.

Our data suggest that the mechanism of Num1 assembly is conserved; mitochondria drive the assembly of Num1 clusters, which serve to anchor the organelle as well as dynein to the cell cortex. In addition to serving as a cortical attachment site for dynein, Num1 also alters dynein activity. In *S. cerevisiae*, Num1 is proposed to activate dynein (Lammers and Markus, 2015), and in *S. pombe*, dynein switches from diffusive to directed motion upon cortical attachment (Ananthanarayanan *et al.*, 2013). Thus, by driving the formation of Num1 clusters, mitochondria not only influence where dynein gets anchored in the cell but also dynein activity at the cortex. The exact mechanistic contributions of mitochondria to Num1-mediated dynein anchoring have yet to be determined. Our recent work demonstrates that the role for mitochondria in dynein anchoring extends beyond simply clustering ScNum1 (Schmit *et al.*, 2018); the interaction between mitochondria and ScNum1 likely promotes an arrangement of ScNum1 within a cluster that is competent for dynein anchoring. It is also possible that contact sites formed by Num1 create a unique microenvironment that is favorable for dynein anchoring and function. Going forward, it will be exciting to elucidate the functional and physiological significance of why mitochondria are used to drive the formation of and remain present at cortical attachment sites for dynein. In addition, it will be important to determine whether other cellular activities are regulated by the membrane contact site formed by Num1.

MATERIALS AND METHODS

Strains and plasmids

Strains W303 (*ade2-1*; *leu2-3*; *his3-11, 15*; *trp1-1*; *ura3-1*; *can1-100*), W303 Δ*num1*::*HIS* and W303 *NUM1-yEGFP*::*HIS* (Ping *et al.*, 2016), W303 *fzo1-1* Δ*dnm1*::*HIS* Δ*num1*::*KAN* (Lackner *et al.*, 2013), W303 *PIL1-yEGFP*::*HIS and PIL1-LaG16::CaURA* (Schmit *et al.*, 2018), and W303 *MMR1-AID-FLAG::HYG* Δ*ypt11::NATNT2 TIR1::URA* (*mito*^{AID}; Kraft and Lackner, 2017) were described previously. The *S. pombe* strains used were h+ *leu1-32; adeM216* and h– *leu1-32; adeM210*.

The following plasmids were previously described: pXY142-mitodsRED (mitoRED; Friedman *et al.*, 2011); p414-MET25 and p414-GPD (Mumberg *et al.*, 1995); p414-MET25::yEGFP-Num1 (Lackner *et al.*, 2013); p414-GalL-yEGFP, p414-GPD-Num1CC-GFP, and pET22b His6-T7 (Ping *et al.*, 2016); pFA6a-link-*yEGFP*::*SpHIS5* (pKT128) and pFA6a-link-*yEGFP-KAN* (pKT127; Sheff and Thorn, 2004); pAGL (Veatch *et al.*, 2009); pRJ06 (Jajoo *et al.*, 2016); pHyg-AID*-GFP (Morawska and Ulrich, 2013); pFA6a-natMX6-PADH-3HA (Euroscarf plasmid #P30346; Van Driessche *et al.*, 2005); pYM-N27 and pYM-N15 (Janke *et al.*, 2004); mCherry-AHDL (a gift from Snezhana Oliferenko, King's College London; Zhang *et al.*, 2010); and pWaldo-GFPd modMCS (Chen *et al.*, 2018). mCherry-AHDL was digested with *Rru*I before being transformed into yeast. HDEL-RFP::TRP (ER-red) was modified from HDEL-GFP::TRP (Rossanese *et al.*, 2001) using standard cloning techniques, and the plasmid was digested with *Eco*RV before yeast transformation.

The following *S. cerevisiae* gene deletion strains were obtained by replacing the complete open reading frame (ORF) of the genes with the indicated cassette using PCR-based targeted homologous recombination: Δ*lnp1::KANMX* and Δ*kar9::HIS* (Longtine *et al.*, 1998; Janke *et al.*, 2004). Haploid double-mutant/tagged strains were generated by backcrossing and tetrad dissection.

GalL::*SpNUM1-yEGFP* and GPD::*SpNUM1-yEGFP* were inserted at the *ScNUM1* endogenous locus in multiple steps. PCR products containing either the coding region of SpNum1 or the yEGFP::KAN cassette with homologous ends were amplified from genomic DNA or pKT127, respectively. The two PCR products were cotransformed into W303 Δ*num1*::*HIS*, resulting in *SpNUM1-yEGFP*::*KAN*. The GalL or GPD promoter was then placed upstream in the genome by PCR-based homologous recombination using pYM-N27 or pYM-N15, respectively, resulting in NAT::GalL::*SpNUM1-yEGFP*::*KAN* and NAT::GPD::*SpNUM1-yEGFP*::*KAN*. To create pAGL::NAT NAT::GalL::*SpNUM1-yEGFP*::*KAN*, NAT::GalL::*SpNUM1-yEGFP*::*KAN* was backcrossed to W303 pAGL, followed by sporulation and tetrad analysis. pAGL encodes for *GAL4-EstrogenBD-VP16*::*NATMX6*, which is the transcription factor used for estradiol control of GAL promoters and integrates at the *LEU2* locus following *Mss*1 digestion (Veatch *et al.*, 2009).

SpNUM1(132-360)-yEGFP was inserted at the *ScNUM1* endogenous locus by cotransforming two PCR products containing either the coding region of *SpNUM1(132-360)* or the *yEGFP*::*KAN* cassette with homologous ends amplified from genomic DNA or pKT127, respectively, into W303 Δ*num1*::*HIS*.

The following *S. pombe* gene deletion strains were obtained by replacing the complete ORF of the genes with the indicated cassette using PCR-based targeted homologous recombination: Δ*dhc1::NATNT2*, Δ*mmb1::NATNT2*, Δ*dnm1::NATNT2*, and Δ*mmb1::KANMX* (Longtine *et al.*, 1998; Janke *et al.*, 2004). The functional C-terminally tagged strains *SpNUM1-yEGFP*::*KAN and DHC1-yEGFP*::*NAT* were constructed by PCR-based targeted homologous recombination using pKT127 and pFA6-link-*yEGFP-NATMX6*. Haploid double-mutant/tagged strains were generated by sequential transformations.

p414-MET25-SpNum1-yEGFP was made by PCR amplifying SpNum1-yEGFP from genomic DNA and cloning into p414-MET25 using *Bam*HI and *Xho*I sites.

pET22b His6-T7-SpNum1 was created by cloning the SpNum1 coding region, amplified from genomic DNA, into pET22b His6-T7 using *Bam*HI and *Xho*I sites.

p414-GPD-ScNum1, p414-GPD-SpNum1, p414-GPD-SpNum1-yEGFP, p414-GPD-SpNum1ΔPH-yEGFP, and p414-GPD-SpNum1ΔCC-yEGFP were constructed by subcloning the respective coding regions into p414-GPD-Num1CC-GFP using *Bam*HI and *Xho*I sites. The coding regions were amplified from p414-MET25::yEGFP-Num1, pET22b His6-T7-SpNum1, p414-MET25-SpNum1-yEGFP, and genomic DNA. Plasmids were then transformed into W303 *fzo1-1* Δ*dnm1*::HIS Δ*num1*::KAN cells. Expression of the GFP constructs was confirmed by Western blot.

To construct p414-GalL-SpNum1(132-360)-yEGFP, SpNum1(132-360)-yEGFP was PCR amplified from genomic DNA and cloned into p414-GalL-yEGFP using *Bam*HI and *Xho*I sites. The plasmid was then transformed into Δ*num1*::HIS pAGL::NAT *PIL1-LaG16::CaURA* cells.

To construct pWaldo SpNum1(132-360)-GFP-His8, SpNum1 (132-360) was PCR amplified from pET22b His6-T7-SpNum1 and cloned into pWaldo-GFPd modMCS using *Bam*HI and *Xho*I sites.

pFA6-link-yEGFP-NATMX6 was constructed by PCR amplifying the NATMX6 cassette from pFA6a-natMX6-PADH-3HA and cloning the product into pKT128 using *Bgl*II and *Eco*RI sites.

mitoRED::HYG was made in multiple steps. The KAN cassette was subcloned from pKT127 to pRJ06 using *Asc*I and *Eco*RI sites, resulting in pRJ06-KAN. The HYG cassette was subcloned from pHyg-AID*-GFP to pRJ06-KAN using *Bgl*II and *Sac*I sites, resulting in pRJ06-HYG. The HYG cassette with genome homology was subcloned from pRJ06-HYG to pRJ06 using *Xho*I and *Sac*I sites, resulting in mitoRED::HYG. This plasmid was digested with *Not*I before being transformed.

Imaging

For Figures 1, B–E, and 2, A and B, all indicated cells harboring mitoRED were grown to mid–log phase in synthetic complete (SC) medium-leucine (SC-LEU) + 2% (wt/vol) dextrose media with 2X adenine. For Supplemental Figure S1, cells were grown in SC + 2% (wt/vol) dextrose media with 2X adenine. For Figure 1, B–E, and Supplemental Figure S1, 10 nM estradiol was added to the pAGL::NAT NAT::GalL::*SpNUM1-yEGFP::KAN* and Δ*lnp1*::KAN pAGL::NAT NAT::GalL::*SpNUM1-yEGFP::KAN* cultures 5 h before imaging.

For Figure 1F, *mito*^{AID} cells with either *ScNum1-yEGFP::KAN* or pAGL::NAT NAT::GalL::*SpNUM1-yEGFP::KAN* and harboring mitoRED were grown in SC-LEU + 2% (wt/vol) dextrose media with 2X adenine, pH = 6.4, at 30°C for 2 h. *mito*^{AID} cells with pAGL::NAT NAT::GalL::*SpNUM1-yEGFP::KAN* were grown in the presence of 10 nM estradiol during this time. Dimethyl sulfoxide or auxin (α-naphthalene acetic acid; HiMedia), to a final concentration of 1 mM, was added and cells were grown for an additional 3 h at 30°C.

For Figure 2, C and D, Δ*num1*::HIS pAGL::NAT *PIL1-LaG16::CaURA* cells harboring p414-GalL-SpNum1(132-360)-yEGFP or p414-GalL-yEGFP and mitoRED were grown to mid–log phase in synthetic complete medium-leucine-tryptophan (SC-LEU-TRP) + 2% (wt/vol) dextrose media with 2X adenine in the presence of 10 or 0.05 nM estradiol, respectively, for 5 h before imaging.

For all *S. cerevisiae* imaging, cells were grown as described above at 24°C unless otherwise indicated, concentrated by centrifugation, and mounted on a 4% wt/vol agarose pad. For all *S. pombe* imaging, haploid cells of the same genotype and opposite mating types were patched over each other on mating plates (1% [wt/vol] dextrose, 7.3 nM KH_2PO_4, 1X vitamins, 0.2X supplements, 3% [wt/vol] agar) and grown at room temperature for 24 h before imaging. Cells were resuspended in a small volume of water and mounted on a 4% wt/vol agarose pad.

All imaging was performed at 22°C. Z series of cells were imaged at a single time point or over time using a spinning disk confocal system (Leica) fit with a spinning disk head (CSU-X1; Yokogawa), a PLAN APO 100× 1.44 NA objective (Leica), and an electron-multiplying charge-coupled device camera (Evolve 512 Delta; Photometrics). A step size of 0.4 µm was used. Image capture was done using Metamorph (Molecular Devices). The images were deconvolved using AutoQuant X3's (Media Cybernetics) iterative, constrained 3D deconvolution method. Fiji (National Institutes of Health) and Photoshop (Adobe) were used to make linear adjustments to brightness and contrast. Deconvolved images are shown.

Image quantification

For Figures 1C and 2, C and D, five-pixel-wide lines were drawn around the circumference of cells in Fiji. The intensities along the line in the red channel were exported to Excel (Microsoft). The number of data points with red fluorescence above background over the total number of data points along the cortex was plotted.

For Figure 1E, five-pixel-wide lines of >7 µm were drawn around the circumference of cells in Fiji for regions with and without GFP clusters. The intensities along the line in both the red and green channels were exported to Excel. The intensity values for regions without GFP clusters were averaged to define a background fluorescence cutoff for each channel and for each genotype. For the regions with GFP clusters, data points with GFP fluorescence above background were scored as having correlated red fluorescence or not. The number of data points with both red and green fluorescence over the total number of data points with green fluorescence was plotted.

For Figure 1F, large buds with a bud/mother diameter ratio of ≥1/3 were scored as having GFP clusters in the bud or not.

For Figure 2, A and B, lines were drawn through a region of interest in Fiji. Intensity profiles across the line were generated for both the red and green channels and were exported to Excel. The data were normalized so that the peak intensity for each channel was set to 1. The position of peak mitoRED intensity was set at 0 µm. The mean intensity and SD were generated for all lines and plotted.

For Figure 3, A and B, and Supplemental Figure S3, SpNum1 clusters and tether points were quantified for a single midslice of wild-type and Δ*dhc1* cells. To be considered a tether point, mitochondria had to remain associated with an SpNum1 cluster for at least three frames of imaging (>1.5 min). A cluster is defined as an accumulation of Num1 above the background signal that persists for at least three frames of imaging (>1.5 min; Kraft and Lackner, 2017). In addition to clusters, Num1 is observed in less intense accumulations as well as in unassembled pools that have a diffuse localization along the cell cortex, neither of which meet the cluster definition. The less intense accumulations of Num1 are dynamic and do not persist over multiple frames.

For Figure 3D, elliptic regions were drawn at the poles of wild-type, Δ*dnm1,* and Δ*mmb1* cells. The total fluorescence intensity for the red and green channels in sum projections was measured and exported to Excel. The fluorescence was normalized to the size of the ellipse. For each genotype, the maximum fluorescence for each channel was set to 1. The data points were plotted as normalized fluorescence intensity of each channel, and the Pearson correlation coefficient was calculated using Prism (GraphPad).

For Figure 3E, SpNum1 clusters and tether points were quantified for a single midslice of wild-type, Δ*dnm1*, and Δ*mmb1* cells. To be considered a tether point, mitochondria had to remain associated with an SpNum1 cluster for at least three frames of imaging (>1.5 min). A cluster is defined as an accumulation of Num1 above the background signal that persists for at least three frames of imaging (>1.5 min). Then, five-pixel-wide lines of >7 µm were drawn around the cortex at the poles of cells in Fiji. The intensities along the line in the red channel were exported to Excel. The number of data points with red fluorescence above background over the total number of data points along the pole cortex was plotted versus the number of clusters at the same pole. Pearson correlation coefficient was calculated using Prism.

For Figure 4, cortical dynein foci at the pole in the direction of the moving spindle pole body that eventually colocalize with the spindle pole body were scored as being mitochondria associated or not within individual slices.

For Supplemental Figure S1, five-pixel-wide lines were drawn around the circumference of cells in Fiji. The intensities along the line in both the red and green channels were exported to Excel. The data were normalized so that the peak intensity for each channel was set to 1.

Protein purification

SpNum1(132-360) was purified from *E. coli* as follows: starter cultures of BL21(λDE3)/RIPL cells harboring plasmids pWaldo SpNum1(132-360)-GFP-His8, from which the expression of the genes is driven by the T7 promoter**,** were grown overnight in Luria-Bertani (LB) medium with chloramphenicol (25 µg/ml), glucose (0.04%), and kanamycin (50 µg/ml). The starter cultures were used to inoculate 2 l of LB medium containing the same additions described above. The cells were grown at 37°C until an OD_{600} of 0.5 was reached. To induce protein expression, isopropyl β-D-1-thiogalactopyranoside (IPTG) was added to a final concentration of

250 µM, and the cultures were grown for 16 h at 18°C. The cells were then harvested by velocity centrifugation at 5000 × *g* for 15 min. The resulting pellet was resuspended in 1/200 volume of resuspension buffer (RB; 20 mM Tris, pH 8.0, 500 mM NaCl, 1.89 mM BME, 1X protease inhibitor cocktail set 1 [PIC; Millipore]), quickly frozen in liquid N_2, and stored at –80°C. The cell suspension was quickly thawed in a room temperature water bath, PIC was added to 1X, and the thawed cell suspension was subjected to two more freeze–thaw cycles. The homogenate was sonicated briefly to further lyse cells and clarified by centrifugation at 17,000 × *g* for 45 min at 4°C. The proteins were purified from the supernatant using HisPur Ni-NTA resin (Thermo Scientific). The supernatant was incubated with resin for 45 min at 4°C, and the resin was then pelleted at 3000 × *g* for 3 min. The protein bound resin was washed three times with RB and three times with wash buffer (RB + 30 mM imidazole + 0.25X PIC) and was then loaded into a chromatography column. Protein was eluted from the column using a step gradient of RB + (60–300) mM imidazole. Five microliters of each elution was mixed with sample buffer, run on a SDS–PAGE gel, and Coomassie stained. Elutions were pooled and dialyzed overnight in 20 mM Tris, pH 8.0, 500 mM NaCl. Glycerol was added to 10%, and the protein was aliquoted, frozen in liquid N_2, and stored at –80°C. The concentration of the purified proteins was determined using a BCA protein assay kit (Pierce).

Liposome flotation assays

Phospholipids were supplied in chloroform from Avanti Polar Lipids. For soybean + 6% CL liposomes, soybean lipid polar extract was mixed with tetraoleoyl-cardiolipin (CL) to achieve a final mol% of 6% CL. For soybean + 0% CL and soybean + 17% CL, compensatory changes were made in the percentage of soybean present in the lipid mixture. For soybean + 34% PA, 34% PS, or 34% PG liposomes, soybean lipid polar extract was mixed with 1-palmitoyl-2-oleoyl-*sn*-glycero-3-phosphate (PA), 1-palmitoyl-2-oleoyl-*sn*-glycero-3-[phosphor-L-serine] (PS), or 1,2-dioleoyl-*sn*-glycero-3-phospho-(1′-rac-glycerol) (PG) to achieve a final mol% of 34% of the indicated lipid. Headgroup-labeled lissamine rhodamine B phosphatidylethanolamine (Rd-PE) was added to all liposome mixtures in trace amounts.

Lipid mixtures were placed in a vacuum chamber overnight. The lipid films were rehydrated with 20 mM HEPES, pH 7.0, to a final lipid concentration of 2 mg/ml at room temperature for 1 h. Lipid mixtures were pipetted up and down to create a heterogeneous population of liposomes. Purified proteins and liposomes, as indicated, were added to gradient reaction buffer (GRB; 20 mM HEPES, pH 7.0, and 150 mM NaCl) for a total volume of 100 µl. This reaction was left at room temperature for 20 min. Sucrose (400 µl of 50%) in GRB was added to the reaction mixture and added to the bottom of a 13 × 51 mm polycarbonate centrifuge tube (Beckman). The reaction plus sucrose mixture was overlaid with 1 ml of 30% sucrose in GRB, 500 µl of 10% sucrose in GRB, and 250 µl of 0% sucrose in GRB for a total volume of 2.5 ml. Sucrose gradients were subjected to centrifugation in a Beckman SW55 rotor at 200,000 × *g* at 4°C for 2 h. Two 1.25 ml fractions were pipetted from the top, resulting in a top and bottom fraction. To monitor the efficiency of the liposome floats, the rhodamine fluorescence of each fraction was quantified using a SpectraMax M5 plate reader (Molecular Devices) with the excitation and emission monochromators set at 550 and 590 nm, respectively. In all cases, >85% of liposomes were observed in the top fraction. To quantify the fraction of protein that floated with the liposomes, equal volumes of top and bottom fractions were analyzed by SDS–PAGE followed by Western analysis using anti-GFP (Invitrogen) for the primary antibody and goat anti-rabbit immunoglobulin G DyLight 800 (Thermo Fisher Scientific) for the secondary antibody. The immunoreactive bands were detected with the Odyssey Infrared Imaging System (Li-Cor Biosciences) and quantified using the accompanying software.

Growth assay

For analysis of growth by serial dilution, cells were grown overnight in synthetic complete medium–tryptophan (SC-TRP) + 2% (wt/vol) dextrose, pelleted, and resuspended in water at a concentration of 0.2 OD_{600}/ml, and 10-fold serial dilutions were performed. Cells were spotted onto casamino acid–TRP + DEX medium and were grown at the indicated temperature.

ACKNOWLEDGMENTS

We thank members of the Lackner lab, Jennifer Brace, members of the Weiss lab, and the WiLa ICB for suggestions and critical scientific discussions. We thank Heidi Schmit-Anderson for help with graphing in R. We thank Yoko Shibata and Rick Morimoto for *S. pombe* strains and advice, Rishi Jajoo for sharing plasmid pRJ06, Snezhana Oliferenko for sharing plasmid mCherry-AHDL, and Jessica Hornick and instrumentation support from the Biological Imaging Facility at Northwestern University. L.M.K. is supported by National Institutes of Health National Institute of General Medical Sciences (NIH NIGMS) Training Grant no. T32GM-008061. L.L.L. is supported by NIH NIGMS Grant no. R01GM-120303 and the Robert H. Lurie Comprehensive Cancer Center–The Lefkofsky Family Foundation/Liz and Eric Lefkofsky Innovation Research Award.

REFERENCES

Adames NR, Cooper JA (2000). Microtubule interactions with the cell cortex causing nuclear movements in *Saccharomyces cerevisiae*. J Cell Biol 149, 863–874.

Ananthanarayanan V, Schattat M, Vogel SK, Krull A, Pavin N, Tolic-Norrelykke IM (2013). Dynein motion switches from diffusive to directed upon cortical anchoring. Cell 153, 1526–1536.

Bleazard W, McCaffery JM, King EJ, Bale S, Mozdy A, Tieu Q, Nunnari J, Shaw JM (1999). The dynamin-related GTPase Dnm1 regulates mitochondrial fission in yeast. Nat Cell Biol 1, 298–304.

Cerveny KL, Studer SL, Jensen RE, Sesaki H (2007). Yeast mitochondrial division and distribution require the cortical Num1 protein. Dev Cell 12, 363–375.

Chang SC, Heacock PN, Clancey CJ, Dowhan W (1998). The *PEL1* gene (renamed PGS1) encodes the phosphatidylglycero-phosphate synthase of *Saccharomyces cerevisiae*. J Biol Chem 273, 9829–9836.

Chao JT, Wong AK, Tavassoli S, Young BP, Chruscicki A, Fang NN, Howe LJ, Mayor T, Foster LJ, Loewen CJ (2014). Polarization of the endoplasmic reticulum by ER-septin tethering. Cell 158, 620–632.

Chen S, Liu D, Finley RL, Greenberg ML (2010). Loss of mitochondrial DNA in the yeast cardiolipin synthase crd1 mutant leads to up-regulation of the protein kinase Swe1p that regulates the G2/M transition. J Biol Chem 285, 10397–10407.

Chen W, Ping HA, Lackner LL (2018). Direct membrane binding and self-interaction contribute to Mmr1 function in mitochondrial inheritance. Mol Biol Cell 29, 2346–2357.

Connerth M, Tatsuta T, Haag M, Klecker T, Westermann B, Langer T (2012). Intramitochondrial transport of phosphatidic acid in yeast by a lipid transfer protein. Science 338, 815–818.

Costanzo M, Baryshnikova A, Bellay J, Kim Y, Spear ED, Sevier CS, Ding H, Koh JL, Toufighi K, Mostafavi S, *et al*. (2010). The genetic landscape of a cell. Science 327, 425–431.

Eshel D, Urrestarazu LA, Vissers S, Jauniaux JC, van Vliet-Reedijk JC, Planta RJ, Gibbons IR (1993). Cytoplasmic dynein is required for normal nuclear segregation in yeast. Proc Natl Acad Sci USA 90, 11172–11176.

Farkasovsky M, Kuntzel H (1995). Yeast Num1p associates with the mother cell cortex during S/G2 phase and affects microtubular functions. J Cell Biol 131, 1003–1014.

Farkasovsky M, Kuntzel H (2001). Cortical Num1p interacts with the dynein intermediate chain Pac11p and cytoplasmic microtubules in budding yeast. J Cell Biol 152, 251–262.

Fridy PC, Li Y, Keegan S, Thompson MK, Nudelman I, Scheid JF, Oeffinger M, Nussenzweig MC, Fenyo D, Chait BT, *et al*. (2014). A robust pipeline for rapid production of versatile nanobody repertoires. Nat Methods 11, 1253–1260.

Friedman JR, Lackner LL, West M, DiBenedetto JR, Nunnari J, Voeltz GK (2011). ER tubules mark sites of mitochondrial division. Science 334, 358–362.

Fu C, Jain D, Costa J, Velve-Casquillas G, Tran PT (2011). Mmb1p binds mitochondria to dynamic microtubules. Curr Biol 21, 1431–1439.

Guillou E, Bousquet C, Daloyau M, Emorine LJ, Belenguer P (2005). Msp1p is an intermembrane space dynamin-related protein that mediates mitochondrial fusion in a Dnm1p-dependent manner in *S.pombe*. FEBS Lett 579, 1109–1116.

Heckman DS, Geiser DM, Eidell BR, Stauffer RL, Kardos NL, Hedges SB (2001). Molecular evidence for the early colonization of land by fungi and plants. Science 293, 1129–1133.

Heil-Chapdelaine RA, Oberle JR, Cooper JA (2000). The cortical protein Num1p is essential for dynein-dependent interactions of microtubules with the cortex. J Cell Biol 151, 1337–1344.

Hermann GJ, Thatcher JW, Mills JP, Hales KG, Fuller MT, Nunnari J, Shaw JM (1998). Mitochondrial fusion in yeast requires the transmembrane GTPase Fzo1p. J Cell Biol 143, 359–373.

Hoppins S, Collins SR, Cassidy-Stone A, Hummel E, Devay RM, Lackner LL, Westermann B, Schuldiner M, Weissman JS, Nunnari J (2011). A mitochondrial-focused genetic interaction map reveals a scaffold-like complex required for inner membrane organization in mitochondria. J Cell Biol 195, 323–340.

Jajoo R, Jung Y, Huh D, Viana MP, Rafelski SM, Springer M, Paulsson J (2016). Accurate concentration control of mitochondria and nucleoids. Science 351, 169–172.

Janke C, Magiera MM, Rathfelder N, Taxis C, Reber S, Maekawa H, Moreno-Borchart A, Doenges G, Schwob E, Schiebel E, *et al*. (2004). A versatile toolbox for PCR-based tagging of yeast genes: new fluorescent proteins, more markers and promoter substitution cassettes. Yeast 21, 947–962.

Jourdain I, Gachet Y, Hyams JS (2009). The dynamin related protein Dnm1 fragments mitochondria in a microtubule-dependent manner during the fission yeast cell cycle. Cell Motil Cytoskeleton 66, 509–523.

Klecker T, Scholz D, Fortsch J, Westermann B (2013). The yeast cell cortical protein Num1 integrates mitochondrial dynamics into cellular architecture. J Cell Sci 126, 2924–2930.

Kormanec J, Schaaff-Gerstenschlager I, Zimmermann FK, Perecko D, Kuntzel H (1991). Nuclear migration in *Saccharomyces cerevisiae* is controlled by the highly repetitive 313 kDa NUM1 protein. Mol Gen Genet 230, 277–287.

Kraft LM, Lackner LL (2017). Mitochondria-driven assembly of a cortical anchor for mitochondria and dynein. J Cell Biol 216, 3061–3071.

Kraft LM, Lackner LL (2018). Mitochondrial anchors: positioning mitochondria and more. Biochem Biophys Res Commun 500, 2–8.

Lackner LL, Ping H, Graef M, Murley A, Nunnari J (2013). Endoplasmic reticulum-associated mitochondria–cortex tether functions in the distribution and inheritance of mitochondria. Proc Natl Acad Sci USA 110, E458–E467.

Lammers LG, Markus SM (2015). The dynein cortical anchor Num1 activates dynein motility by relieving Pac1/LIS1-mediated inhibition. J Cell Biol 211, 309–322.

Lemmon MA 2010. Pleckstrin homology (PH) domains. In: Handbook of Cell Signaling, 2nd ed., ed. EA Dennis, San Diego: Academic Press, 1093–1101.

Longtine MS, McKenzie A 3rd, Demarini DJ, Shah NG, Wach A, Brachat A, Philippsen P, Pringle JR (1998). Additional modules for versatile and economical PCR-based gene deletion and modification in *Saccharomyces cerevisiae*. Yeast 14, 953–961.

Markus SM, Lee WL (2011). Regulated offloading of cytoplasmic dynein from microtubule plus ends to the cortex. Dev Cell 20, 639–651.

Mata J, Lyne R, Burns G, Bähler J (2002). The transcriptional program of meiosis and sporulation in fission yeast. Nat Genet 32, 143–147.

McFaline-Figueroa JR, Vevea J, Swayne TC, Zhou C, Liu C, Leung G, Boldogh IR, Pon LA (2011). Mitochondrial quality control during inheritance is associated with lifespan and mother-daughter age asymmetry in budding yeast. Aging Cell 10, 885–895.

Miller RK, Rose MD (1998). Kar9p is a novel cortical protein required for cytoplasmic microtubule orientation in yeast. J Cell Biol 140, 377–390.

Morawska M, Ulrich HD (2013). An expanded tool kit for the auxin-inducible degron system in budding yeast. Yeast 30, 341–351.

Mumberg D, Muller R, Funk M (1995). Yeast vectors for the controlled expression of heterologous proteins in different genetic backgrounds. Gene 156, 119–122.

Muyldermans S (2013). Nanobodies: natural single-domain antibodies. Annu Rev Biochem 82, 775–797.

Pernice WM, Swayne TC, Boldogh IR, Pon LA (2017). Mitochondrial tethers and their impact on lifespan in budding yeast. Front Cell Dev Biol 5, 120.

Pernice WM, Vevea JD, Pon LA (2016). A role for Mfb1p in region-specific anchorage of high-functioning mitochondria and lifespan in *Saccharomyces cerevisiae*. Nat Commun 7, 10595.

Ping HA, Kraft LM, Chen W, Nilles AE, Lackner LL (2016). Num1 anchors mitochondria to the plasma membrane via two domains with different lipid binding specificities. J Cell Biol 213, 513–524.

Ren G, Vajjhala P, Lee JS, Winsor B, Munn AL (2006). The BAR domain proteins: molding membranes in fission, fusion, and phagy. Microbiol Mol Biol Rev 70, 37–120.

Rossanese OW, Reinke CA, Bevis BJ, Hammond AT, Sears IB, O'Connor J, Glick BS (2001). A role for actin, Cdc1p, and Myo2p in the inheritance of late Golgi elements in *Saccharomyces cerevisiae*. J Cell Biol 153, 47–62.

Saito TT, Okuzaki D, Nojima H (2006). Mcp5, a meiotic cell cortex protein, is required for nuclear movement mediated by dynein and microtubules in fission yeast. J Cell Biol 173, 27–33.

Schmit HL, Kraft LM, Lee-Smith CF, Lackner LL (2018). The role of mitochondria in anchoring dynein to the cell cortex extends beyond clustering the anchor protein. Cell Cycle 17, 1–13.

Schwarz TL (2013). Mitochondrial trafficking in neurons. Cold Spring Harb Perspect Biol 5, a011304.

Sheff MA, Thorn KS (2004). Optimized cassettes for fluorescent protein tagging in *Saccharomyces cerevisiae*. Yeast 21, 661–670.

Sheng ZH (2017). The interplay of axonal energy homeostasis and mitochondrial trafficking and anchoring. Trends Cell Biol 27, 403–416.

Simbeni R, Pon L, Zinser E, Paltauf F, Daum G (1991). Mitochondrial membrane contact sites of yeast. Characterization of lipid components and possible involvement in intramitochondrial translocation of phospholipids. J Biol Chem 266, 10047–10049.

Sipiczki M (2000). Where does fission yeast sit on the tree of life? Genome Biol 1, reviews1011.1–1011.4.

Tang X, Germain BS, Lee WL (2012). A novel patch assembly domain in Num1 mediates dynein anchoring at the cortex during spindle positioning. J Cell Biol 196, 743–756.

Tang X, Punch JJ, Lee WL (2009). A CAAX motif can compensate for the PH domain of Num1 for cortical dynein attachment. Cell Cycle 8, 3182–3190.

Thankachan JM, Nuthalapati SS, Addanki Tirumala N, Ananthanarayanan V (2017). Fission yeast myosin I facilitates PI(4,5)P2-mediated anchoring of cytoplasmic dynein to the cortex. Proc Natl Acad Sci USA 114, E2672–E2681.

Van Driessche B, Tafforeau L, Hentges P, Carr AM, Vandenhaute J (2005). Additional vectors for PCR-based gene tagging in *Saccharomyces cerevisiae* and *Schizosaccharomycespombe* using nourseothricin resistance. Yeast 22, 1061–1068.

Veatch JR, McMurray MA, Nelson ZW, Gottschling DE (2009). Mitochondrial dysfunction leads to nuclear genome instability via an iron-sulfur cluster defect. Cell 137, 1247–1258.

Walther TC, Brickner JH, Aguilar PS, Bernales S, Pantoja C, Walter P (2006). Eisosomes mark static sites of endocytosis. Nature 439, 998–1003.

Yamamoto A, Tsutsumi C, Kojima H, Oiwa K, Hiraoka Y (2001). Dynamic behavior of microtubules during dynein-dependent nuclear migrations of meiotic prophase in fission yeast. Mol Biol Cell 12, 3933–3946.

Yamamoto A, West RR, McIntosh JR, Hiraoka Y (1999). A cytoplasmic dynein heavy chain is required for oscillatory nuclear movement of meiotic prophase and efficient meiotic recombination in fission yeast. J Cell Biol 145, 1233–1249.

Yamashita A, Yamamoto M (2006). Fission yeast Num1p is a cortical factor anchoring dynein and is essential for the horse-tail nuclear movement during meiotic prophase. Genetics 173, 1187–1196.

Yu JW, Mendrola JM, Audhya A, Singh S, Keleti D, DeWald DB, Murray D, Emr SD, Lemmon MA (2004). Genome-wide analysis of membrane targeting by *S. cerevisiae* pleckstrin homology domains. Mol Cell 13, 677–688.

Zhang D, Vjestica A, Oliferenko S (2010). The cortical ER network limits the permissive zone for actomyosin ring assembly. Curr Biol 20, 1029–1034.

Zinser E, Daum G (1995). Isolation and biochemical characterization of organelles from the yeast, *Saccharomyces cerevisiae*. Yeast 11, 493–536.